Surface Science 644 (2016) 180–190

Contents lists available at ScienceDirect

Surface Science

journal homepage: www.elsevier.com/locate/susc

In-situ infrared study of silicon in KOH electrolyte: Surface hydrogenation and hydrogen penetration

H.G.G. Philipsen [a,b,1], F. Ozanam [b], P. Allongue [b], J.J. Kelly [a], J.-N. Chazalviel [b,*]

[a] Debye Institute for Nanomaterials Science, Utrecht University, P.O. Box 80000, 3508 TA, Utrecht, The Netherlands
[b] Physique de la Matière Condensée, CNRS-Ecole Polytechnique, 91128 Palaiseau, France

ARTICLE INFO

Article history:
Received 6 August 2015
Accepted 24 October 2015
Available online 2 November 2015

Keywords:
Hydrogen in semiconductors
Band bending
Silicon surface chemistry
Anisotropic etching
Surface states
Free-carrier absorption

ABSTRACT

The n-Si(111)/6 M KOH electrolyte interface has been investigated by *in-situ* multiple-internal reflection infrared spectroscopy, at room temperature and at 40 °C. The potential of the Si electrode was stepped successively to positive and negative values with respect to open-circuit potential, leading to surface oxidation and oxide dissolution, respectively. Infrared spectra were recorded together with the interfacial current. Analysis of the infrared spectra indicates that, following the positive potential step, the electronic state of the surface changes from accumulation to inversion and the surface termination changes from a hydrogenated state to an oxidised state. The hydrogenated state is recovered after an induction time following the negative potential step. However, hydrogen penetration into the silicon lattice is then found to take place, as indicated by the appearance of a new SiH band and a strong background absorption of electronic origin. This sub-surface hydrogenation is associated with a slow increase of the interfacial current. This process is found to be especially important at higher temperature and is attributed to the formation of microcracks partially decorated with hydrogen. These results indicate that the chemistry and morphology of a silicon electrode are not stable even in the presence of an applied negative potential.

1. Introduction

The striking orientation dependence of the chemical etching of Si in alkaline solutions forms the basis for important applications in Micro-Electro-Mechanical Systems (MEMS). The key feature here is the very low etch rate of the Si(111) surface [1–4]. On the other hand, anodic passivation of Si in alkaline solution has proved important in the field of etch-stop techniques, widely used in the fabrication of beams, membranes, and other components in MEMS devices [5,6]. These two properties have been successfully exploited in device technology [5,6].

At open-circuit potential (OCP) in alkaline solution, Si undergoes chemical dissolution giving, as products, silicate in solution and hydrogen gas [1,3,6,7]. Surprisingly, *in-situ* and *ex-situ* infrared (IR) spectroscopy has shown that, during chemical etching in NaOH and KOH solution, the surface of Si is hydrogen terminated [8–10]. The electrochemistry of p-type Si in alkaline medium looks straightforward. When the potential is scanned positive of OCP, oxidation by surface holes gives rise to an anodic current peak followed by surface passivation [11–13]. In the range negative of OCP, the cathodic current is low because of the absence of electrons in the conduction band in the dark, and the chemical etch rate is close to that measured at OCP [13,14]. For the case of n-Si, at potentials negative of OCP, a cathodic current results from hydrogen evolution due to conduction-band electrons, and the etch rate is reduced [11–13]. *In-situ* STM studies in NaOH solution showed the (111) surface to consist of atomically flat terraces with the (1 × 1)-H structure separated by bilayer steps [10]. At potentials negative of OCP, perfect step-flow etching is observed. At OCP, dissolution proceeds via step flow and, to a lesser extent, by pitting on the terraces [10]. Surprisingly, when the potential is scanned positive of OCP in the dark, a current peak comparable to that on p-Si is also observed, despite the absence of valence band holes [11,12,15]. This anodic current has been attributed to electron injection into the conduction band from surface states associated with intermediates of the chemical etching reaction [10,12,13]. There is evidence that electron injection also occurs to some extent with p-Si [12]. In both cases, chemical etching is suppressed as soon as anodic passivation occurs [4,12,14].

Clearly, the surface chemistry of Si in aqueous solution of high pH is complex. In an attempt to clarify the mechanisms of anodic oxidation and oxide dissolution, we have undertaken an *in-situ* IR study of these processes. In KOH and NaOH solution, chemical etching of Si(100) and Si(110) is fast and tends to give roughened surfaces [1,3,4], not suitable for an extended IR study. Consequently, we used the Si(111) surface which has added advantages for a spectroscopic investigation of anodic processes: the chemical etch rate is very low and as a result the rate of evolution of hydrogen bubbles from the surface is limited. Previous studies involving potential-step measurements with n-Si(111) have

* Corresponding author at: 25 rue Eugène Combes, 19800 Corrèze, France.
E-mail address: jean-noel.chazalviel@polytechnique.edu (J.-N. Chazalviel).
[1] Present address: IMEC, Kapeldreef 75, Leuven, Belgium.

http://dx.doi.org/10.1016/j.susc.2015.10.040
0039-6028/

shown an unexpectedly long induction time for oxide film formation, a feature attractive for kinetic studies [11,15]. These various considerations led us to the choice of atomically flat n-Si(111) as the starting electrode for our study. The electrode potential was stepped repeatedly between a negative value, at which hydrogen was evolved, and a potential in the passive range, at which surface oxide was formed. In addition, the use of an n-type electrode allowed us to study the surface chemistry during the cathodic generation of hydrogen at the negative potential.

In the present paper, we describe our experiments performed in 6 M KOH solution at room temperature (RT) and 40 °C. We focus on three topics: i) changes in the electronic properties of the surface during potential cycling, as determined from the electronic absorption baseline in the IR spectra; ii) the role of hydrogen at the surface, *i.e.* oxidation and regeneration of the hydrogen-terminated surface; and iii) interaction of hydrogen with the silicon crystal. The results on oxide formation and dissolution will be reported in a companion paper [16].

2. Experimental

The IR spectra were taken in the now classical multiple-internal-reflection geometry [17]. However, the use of KOH electrolyte at temperatures above 25 °C requires the design of a specific cell, which cannot be made of glass. We have made two series of experiments: at room temperature (RT) and at 40 °C (which builds a bridge to the transient studies in the literature). In each case, the experiments were performed in the dark, in a solution of 6 M KOH (VLSI grade from Merck, Selectipur). For the room-temperature experiments, the cell was similar to that used for fluoride electrolytes [18]. Namely, it was made of polytrifluorochloroethylene with a Pt-wire counter electrode. For the 40 °C experiments, the body of the cell was machined in stainless steel, which was also used as the counter electrode. A power resistor (as the heating element) and a Pt-resistance temperature sensor were inserted in the stainless-steel block and the temperature was controlled to ±0.1 °C through a home-designed electronic regulation. Preliminary tests indicated that stainless steel is perfectly stable at open circuit in the operating conditions, and *post-mortem* examination of our silicon samples using XPS analysis did not reveal any trace of metal contamination.

For the two arrangements, the n-Si samples [float-zone grown, ⟨111⟩ orientation, 0.2 ± 0.05° misoriented towards the $\langle 11\bar{2}\rangle$ direction, P-doped, 130–150 Ωcm resistivity, 500 μm thickness, from ITME (Poland)], were shaped as trapezoids (20 × 15 mm², 45° bevels along the longer edges). For sample preparation, a sacrificial anodic area was implemented by scratching the surface in a region outside the IR path. The samples were then cleaned by Piranha/HF cycles and their surface was prepared atomically flat by etching in de-oxygenated NH_4F solution, as described in more detail in [19]. The samples were mounted in the cell by pressing them against a circular aperture in the cell wall with a perfluorinated elastomer 10-mm inner diameter O-ring seal. In this geometry, 10 reflections take place at the Si/electrolyte interface. Two electrical contacts to the sample were made in the upper corners, away from the optical path, by rubbing the surface with In-Ga eutectic and contacting the liquid–metal drop with a copper clip. The mercury/mercurous sulphate reference electrode, to which potentials will be referred in the following, was connected to the cell through a long polytetrafluoroethylene pipe (salt bridge). The electrochemical cell was controlled with a home-made four-electrode potentiostat. The use of two independent contacts for the working electrode (a sensing contact for the potential and the other for current flow) helps to avoid errors in the value of the potential due to poor ohmicity of the contacts and/or series resistance of the Si electrode.

The IR spectra were recorded with a Bruker Equinox 55 spectrometer (800–4500 cm^{-1} spectral range, 4 cm^{-1} resolution). The cell was mounted in a home-designed external compartment, including a rotatable grid polariser and an Infrared Associates MCT liquid-nitrogen cooled photovoltaic detector. The small magnitude of the signals required using accumulation of several interferograms, so that a spectrum could be obtained every 20–30 s. The potential was stepped successively to positive and negative values with respect to open-circuit potential, leading to surface oxidation and oxide dissolution, respectively. Each potential was maintained until the current became stable. The typical duration of such a cycle was 40–50 min at 40 °C and 2–3 h at RT. Infrared spectra were continuously recorded together with the interface current. Several such cycles were run and the results could be either considered separately for checking the reproducibility, or accumulated for improving the signal-to-noise ratio.

The spectra were converted to differential absorbance spectra by choosing a reference state (*e.g.*, the steady state at the negative potential) and calculating $(1/N)\ln[I_0(\sigma)/I(\sigma)]$, where σ is wave number, $N = 10$ is the number of useful reflections at the Si/electrolyte interface, $I_0(\sigma)$ is the raw spectrum in the reference state, and $I(\sigma)$ is the spectrum of interest. Analysis of these differential spectra was performed by using a versatile home-made fitting software. In the following, the fitting methods for each spectral range will be mentioned only briefly, the technical details being given in Appendix A.

3. Results

The results of the experiments at RT and at 40 °C turned out to exhibit marked differences, which were found to be reproducible over many experiments. For that reason, we will present them in two separate subsections.

3.1. The RT study

Fig. 1 shows a typical current transient (Fig. 1a) and the corresponding series of spectra recorded at RT upon stepping the potential from −1.3 V to +1.0 V and back (Fig. 1b). Here the raw IR data actually consisted of 1200 spectra, representing 3 cycles of 400 spectra each. Fig. 1b was obtained by accumulating the three cycles and taking the average of each 5 consecutive spectra. Within each cycle, the reference was taken as the average of the first 40 raw spectra, recorded just before the positive-potential step (taken as the origin of time). It is clear from Fig. 1b that potential cycling leads to many changes in the IR spectra. Among the most conspicuous features are the disappearance of the SiH surface bonds (negative band around 1900–2200 cm^{-1} associated with the formation of an oxide layer (νSiO absorption in the 900–1250 cm^{-1} region) at the positive potential, and the progressive disappearance of the oxide at the negative potential together with the restoration of the SiH surface bonds.[2] One also notices a reversible modification of the baseline. The oxide formation/dissolution will be discussed in detail in a separate paper [16]. Here, we will focus our attention on the changes in the νSiH region (1900–2200 cm^{-1}) and in the baseline. The various contributions considered are listed in Table 1.

3.1.1. Current transients

The current transient following the positive-potential step exhibits a fast and a slow component, like those reported in the literature [11,15]. However, here the current maximum is barely seen. This is plausibly due to the fact that the fast component is dominant, whereas the slow component is reduced in magnitude (~10 μA/cm²) and extends to several hundred seconds. These latter effects can be attributed to the lower temperature (25 °C here as compared to 60 °C in Ref. [15] or 40–70 °C in Ref. [11]).

When the potential is stepped back to the negative bound, there is a weak negative current transient, the cathodic current remains very low (~−1 μA/cm²) for about 1000 s, then it slowly increases, and finally tends to a steady-state value of ~−20 μA/cm² about 7000 s after the

[2] The presence of two weak peaks at 2855 and 2930 cm^{-1} and other features in the 1400–1600 cm^{-1} range is due to the O-ring seal and is discussed in the companion paper [16].

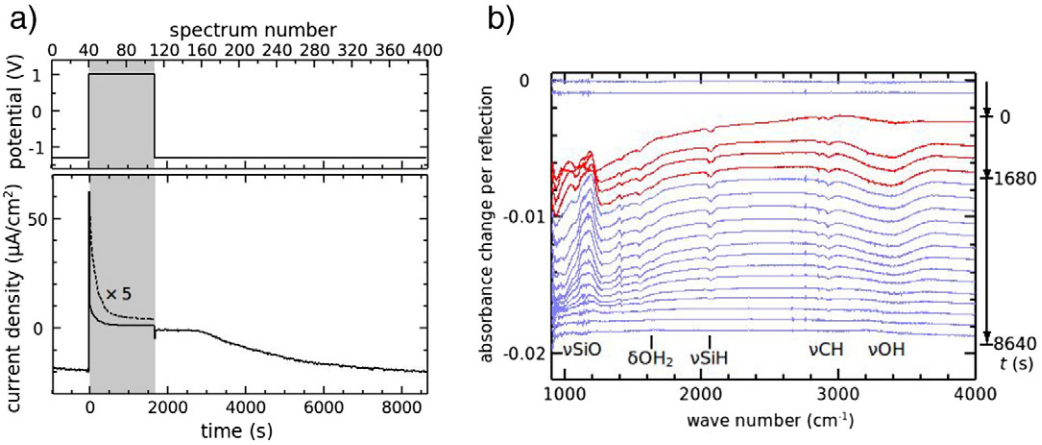

Fig. 1. Typical room-temperature results for n-Si in 6 M KOH solution. (a) Potential cycle and the resulting current transients. The upper scale gives the correspondence between time and spectrum number within a cycle. The grey shading indicates the time spent at the positive potential. (b) Series of IR spectra, recorded in p-polarisation, extracted from the complete data set (3 cycles of 400 spectra each = 1200 spectra). The reference was taken in the steady state at the negative potential. The spectra shown here are the result of a double averaging: average of packets of 5 consecutive spectra, and average of the 3 cycles. For clarity, only one out of 4 such averaged spectra is shown (hence, 400:5:4 = 20 curves). The successive curves have been shifted vertically by increments of −0.001 for clarity (the vertical right-hand scale gives a qualitative indication of the corresponding time). The red (resp. light-blue) lines stand for spectra recorded at the positive (resp. negative) potential. Note the sudden change in baseline following the positive potential step ($t \approx 0$, third spectrum from top).

negative potential step. The origin of this very slow increase will be clarified after the IR spectra are analysed.

3.1.2. νSiH region

Visual inspection of Fig. 1b shows that the positive potential step is followed by a loss in νSiH absorption around 2070 cm^{-1}, and the initial state is progressively recovered some time after the negative potential step. However, a careful examination of the spectra at intermediate stages reveals interesting details: Fig. 2 shows a zoom-in on the νSiH region in p- and s-polarisation at $t = 120$ s (*i.e.*, 120 s after the positive-potential step). The p-polarisation spectrum clearly exhibits two components: a negative one around 2066 cm^{-1} and a positive one around 2120 cm^{-1}, which is weaker. In s-polarisation, the band at 2066 cm^{-1} is very weak. The solid lines in Fig. 2 result from the fit of the spectral decomposition with the above two bands (Gaussian functions) and a second-order polynomial baseline. The shape of this spectrum is typical of those observed throughout the entire potential cycling. Only the absolute and relative band intensities are varying with time.

Fig. 3a presents the time dependence of the two band intensities during potential cycling. The solid lines correspond to p-polarisation and the dashed lines to s-polarisation. The main band SiH(2066) is seen to lose about two thirds of its total intensity at the very first spectrum following the positive potential step; then it decays slowly on a time scale of *ca* 200 s, and a steady-state value is reached, plausibly corresponding to complete removal of the associated species. The extra band SiH(2120), actually centred between 2100 and 2160 cm^{-1} (see Fig. 3b), increases after the positive-potential step, then slowly decreases, though it does not seem to return to zero. Note that the intensity of the SiH(2066) band is strongly polarisation dependent (an order of magnitude stronger in p-polarisation than in s-polarisation), while that of the SiH(2120) band is consistent with a random orientation of the associated dynamic dipole (within experimental uncertainty, which is rather large given the weakness of the signals and the noisy character of the results). The strong polarisation dependence of the SiH(2066) band indicates that it is associated with SiH bonds perpendicular to the surface, as expected indeed at an ideal hydrogen-terminated (111) Si surface [20]. The broadening and downward shift of the band as compared to the values reported in the literature (centre at 2083 cm^{-1} with a FWHM on the order of 1 cm^{-1} [20]) can be attributed to the interaction of the SiH vibrators with the 6 M KOH electrolyte [21]. The survival of a weak contribution in s-polarisation may be due to the presence of step sites associated with pits on the otherwise atomically flat (111) surface. The position of the SiH(2120) band, together with its time dependence, suggests that it arises from SiH species with oxidised silicon backbonds, which play the role of intermediates in the oxidation process, but do not fully disappear at the positive potential.

On the negative-potential step, there is hardly any variation of the SiH(2066) band before a delay on the order of 2000 s, then it slowly increases again, the initial state being recovered after about 5000 s spent at the negative potential. Here again, the SiH(2120) band goes through a

Table 1
Summary of the various contributions considered in analysing the spectra.

Vibrational bands			
Notation	Actual position (cm^{-1})	Assignment	Comments
SiH(2066)	2065.7	νSiH in $(Si_3)SiH$	polarisation sensitive (p > > s)
SiH(2120)	2100–2150	νSiH in $(Si_{3-x}O_x)SiH$	p/s ~ 2
SiH(2000)	1900–2000	νSiH in $(Si_{bulk})H$	40 °C data only; p/s ~ 1

Baseline	
Origin/Notation	Spectral shape
Free electrons/FE	Drude shape ($\propto \omega^{-2}$) + broad Gaussian around 3800 cm^{-1} (interband transition)
Free holes	Drude shape ($\propto \omega^{-2}$)
H inside Si/EL	Exponential tail of a band centred above 4000 cm^{-1}
H inside Si/LL	Lucovsky-like shape (broad maximum around 3000 cm^{-1}); 40 °C data only
Diffusion losses	Contribution independent of wave number

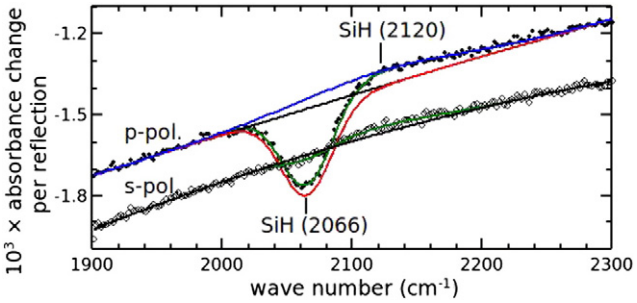

Fig. 2. Fits of the SiH band with a second-order polynomial background plus two Gaussian contributions (here 120 s after the positive-potential step, spectra taken in s- and p-polarisation). Note the strong dependence on IR polarisation and the need for a positive-band contribution for fitting the data (here band centred at around 2120 cm^{-1}).

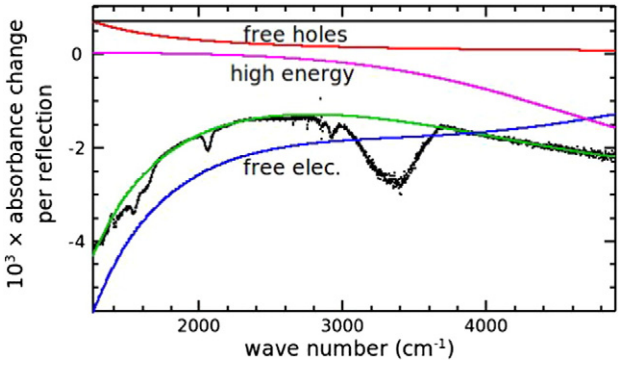

Fig. 4. Typical fit of the baseline, here for spectrum no. 110 ($t = 1680$ s, just before the negative potential step, p-polarisation). The intervals where vibrational bands are present have been excluded from the fit (see text). Free-electron (blue), free-hole (red), "high-energy" (magenta), and "constant" (black) contributions. The black dots represent the data and the green line the fit.

broad maximum at intermediate times. The same polarisation dependences are observed as during the oxidation process. Interestingly, the position of the SiH(2120) band appears to be somewhat higher in the steady state at the positive potential than at intermediate stages (see Fig. 3b). A plausible interpretation is that SiH bonds with one or two oxygen atoms in the silicon backbonds [(OSi_2)SiH and (O_2Si)SiH] may be present (a positive shift of 50–60 cm^{-1} per oxygen is to be expected [22]), and the relative proportion of (O_2Si)SiH increases with the degree of oxidation of the surface.

3.1.3. Baseline absorption

Fig. 4 shows a typical broadband spectrum, here at time $t = 1680$ s, *i.e.* just before the negative-potential step. The baseline was analysed by fitting the spectra in the regions free from vibrational signals, namely, in the union of the intervals (1260–1350 cm^{-1}), (1700–2000 cm^{-1}), (2150–2200 cm^{-1}), and (3700–4900 cm^{-1}), as the superposition of three contributions: a free-carrier contribution, a high-energy contribution, and a "constant" (*i.e.*, wave-number independent, but spectrum dependent) contribution. The presence of a strong negative free-carrier contribution following the positive-potential step is conspicuous from the low-energy sloping background appearing at $t = 0$ (see Fig. 1b). The so-called "high-energy contribution" consists of a weak high-energy tail, which was modelled as a Gaussian with centre at around 6000 cm^{-1} and FWHM 3000 cm^{-1}, a classical spectral shape, *e.g.*, for surface-state absorption [23]. Note that, in the spectral range of interest, this Gaussian shape is close to a simple exponential. Here again, the centre and FWHM were initially left free, then they were frozen at the above values, which represent an average of the results from these fits. The origin of this high-energy contribution, as well as that of the "constant" contribution, will be discussed later.

Fig. 5 summarises the results of the series of fits, obtained from the p-polarised spectra (the s-spectra leading to very similar results). On the positive potential step, there is a sudden drop in free-electron absorption. The negative free-electron contribution appearing in the differential spectra actually corresponds to the disappearance of the strong accumulation layer present at the negative potential, taken as

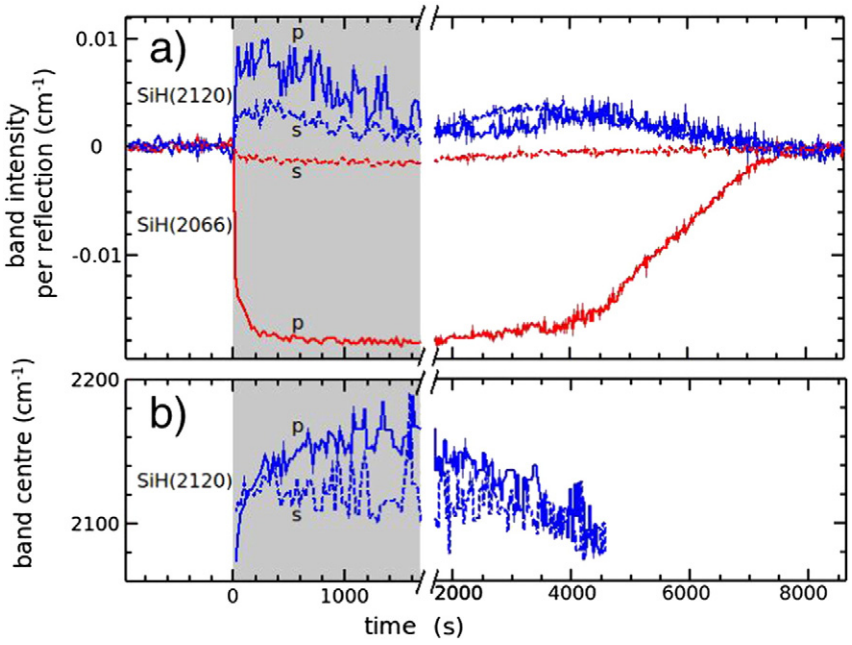

Fig. 3. Results of the analysis of the νSiH region (reference state = steady state at the negative potential). The shaded region indicates the time spent at the positive potential. Note the break in the time scale at $t = 1680$ s (time of the negative-potential step). (a) Variation in the intensity of the two Gaussian bands [SiH(2066) at 2065.7 cm^{-1}, red, and SiH(2120), blue], for the p-polarised (solid lines) and the s-polarised (dashed lines) spectra. Note that the main band is much stronger in p-polarisation than in s-polarisation. (b) Actual position of the SiH(2120) band, as obtained from the fits.

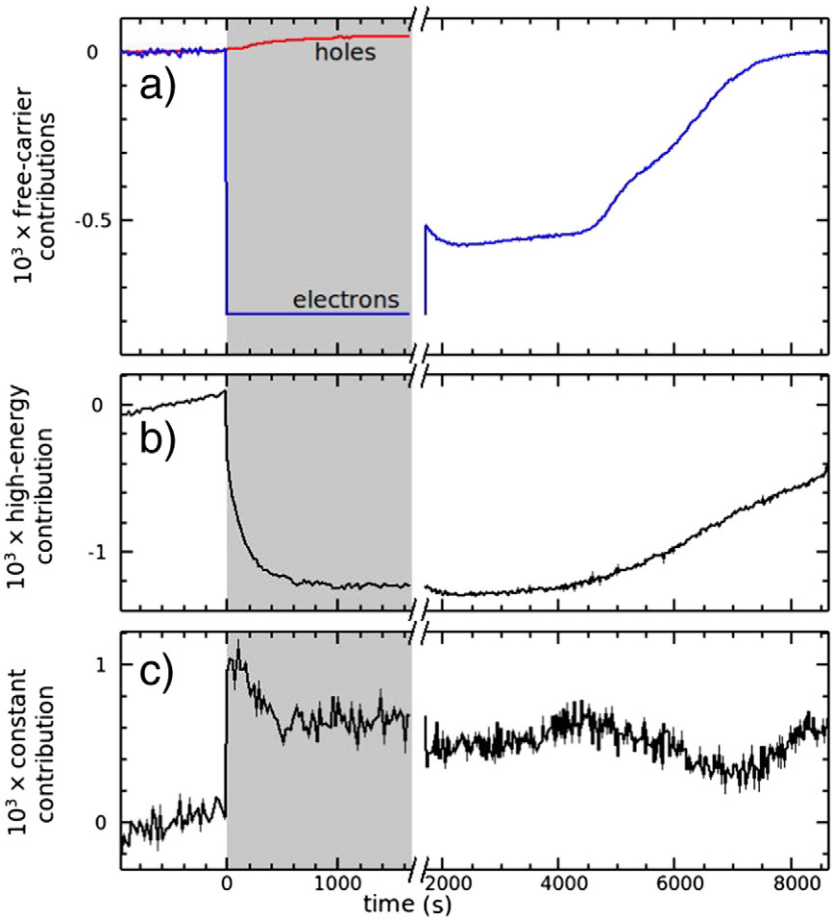

Fig. 5. Variation of the three baseline contributions as a function of time (p-polarisation, referred to the steady state at the negative potential): (a) free-carrier contributions (free holes: specified at 4900 cm^{-1}; free electrons: coefficient of the SF expression given in Appendix A.1); (b) high-energy contribution (specified at 4000 cm^{-1}); (c) constant contribution. The shaded region indicates the time spent at the positive potential. Note the break in the time scale at the time of the negative potential step.

the reference state (hence, the true "zero" of free-electron absorption is the value after the positive potential step). Then an inversion layer is seen to develop on a time scale of 200–400 s, plausibly corresponding to the growth of an oxide layer. The initial free-carrier absorption is partly recovered on the negative-potential step, but full recovery is reached only after a delay, attributable to the time required for oxide dissolution. At the same time as a hole accumulation layer appears, the high-energy absorption steadily decreases. Strangely enough, its initial value is not fully recovered at the end of the cycle; this has been confirmed by analysing the spectra of successive cycles (without accumulation of several cycles, see discussion below). Finally, the "constant" contribution is seen to exhibit an overall increase, superimposed on variations with local maxima at the times when the surface composition is changing (*i.e.*, oxidation at $t = 0$–400 s, and re-hydrogenation around $t = 4000$ s). These features will be discussed below.

3.2. The 40 °C results

The 40 °C results appear rather different from the RT results. As was to be expected, the time scale on which the changes take place is much shorter. The current transients (Fig. 6) indicate that the "slow" component is now dominant and a clear maximum ($\approx$25 μA/cm^2) is seen at around 120 s after the positive-potential step. However, the most striking and surprising change is in the shape and variation of the baseline. For that reason, we will first present the fits of the baseline, then consider the νSiH bands.

3.2.1. Baseline absorption

Fig. 7 shows a typical series of spectra. The baseline appears quite different from that in the RT spectra: i) its magnitude is typically

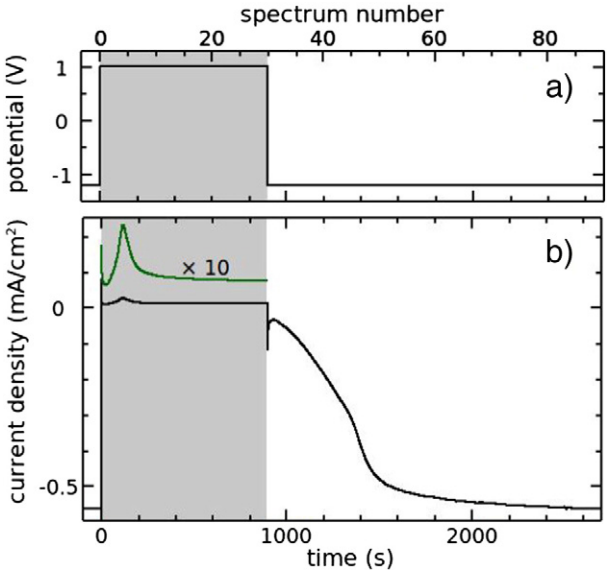

Fig. 6. Typical potential cycle (a) and the resulting current transients (b) for n-Si in 6 M KOH solution at 40 °C. The upper scale gives the correspondence between time and spectrum number within a cycle.

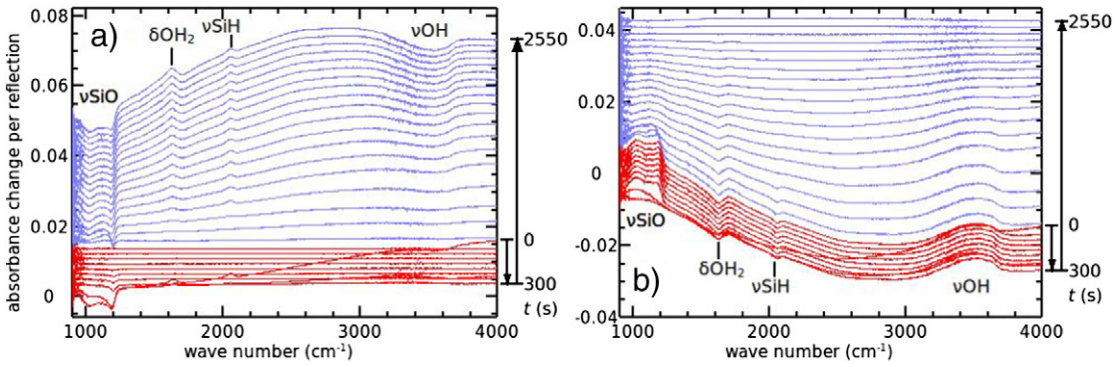

Fig. 7. Series of IR spectra, recorded in p-polarisation. The spectra shown here are the result of averaging over 3 consecutive cycles. Only one averaged spectrum out of 3 is shown, with a vertical shift of 0.0015 per spectrum (red lines for positive potential, light-blue lines for negative potential, qualitative time scale shown at the right). (a) The reference was taken in the steady state at the positive potential. (b) Same data, the reference being taken at the end of the cycle. Note the initial decrease of the baseline at high energy (which leads to the *apparently* non-monotonic time scale on the right-hand side, though the vertical shift is linear as a function of spectrum number) and its irreversible increase through the spectral range while at the negative potential.

10–30 times larger, ii) it does not return to zero at the end of a cycle but instead exhibits a continuous increase while the potential is set at its negative bound, iii) the free-carrier contribution is hardly visible, and iv) the overall shape appears to be governed by a broad contribution peaking at around 3000 cm^{-1}. Due to the irreversible increase of the baseline [point ii) above], the choice of the reference spectrum becomes a problem. For that reason, the spectra in Fig. 7 were displayed by using as a reference spectrum either the average of the last 10 spectra before the negative-potential step (for which the baseline appears stable, Fig. 7a), or the average of the 10 spectra at the end of the cycle (for which the surface is oxide-free but the baseline is steadily increasing, Fig. 7b). In practice, the first representation was used for analysing the baseline, whereas the second was preferred for analysing the vibrational data (since that reference plausibly corresponds to an oxide-free state).

Fig. 8 shows a typical broadband spectrum (p-polarisation, t = 1800 s, reference taken just before the negative potential step). As expected from visual inspection, this baseline cannot be accounted for by the three contributions used for the RT spectra. An additional very broad band centred around 3000 cm^{-1} must be added. This new band is reminiscent of the absorption by deep impurity centres in semiconductors, as predicted by the model of Lucovsky [24]. In the framework of that model, the optical absorption resulting from the transition from the impurity state to the nearest band is described by the optical cross-section $\sigma_{Luc}(\omega) = (4e^2\hbar/3n\varepsilon_0 m^* c)E_i^{1/2}(\hbar\omega - E_i)^{3/2}/(\hbar\omega)^3$, where $\hbar\omega$ is photon energy, E_i is the ionisation threshold, n is the refractive index of the semiconductor, and the other symbols have their usual meanings [24]. This expression indeed exhibits a maximum at $\hbar\omega = 2E_i$ and a slow decrease above this maximum. A further broadening may appear in the presence of atomic reorganisation effects, which result in a blue shift and Gaussian-like distribution of the effective ionisation energy [25]. We have then fitted the baseline as the sum of three contributions: i) a free-electron (FE) contribution, which remains rather weak as compared to the next two contributions, ii) an "exponential-like " (EL) high-energy contribution similar to that used for the RT fits; and iii) a "Lucovsky-like" (LL) contribution (see Appendix A). A typical fit is shown in Fig. 8. Note that the FE contribution is weak and the resulting value bears a large uncertainty.

Fig. 9 shows the results from fitting the series of spectra, averaged over 3 cycles and for s- and p-polarisation. As was to be expected from direct inspection of the spectra, the most conspicuous feature is the predominance of the LL contribution. All three contributions are seen to be quite stable in the steady state at the positive potential (*i.e.*, close to zero since the reference state has been taken just before the negative-potential step). Within the uncertainty of the fits, the FE and EL contributions are seen to recover more or less their initial values at the end of the cycle. In contrast, the LL contribution exhibits a huge increase at the negative potential, and ends at a level much higher than at the beginning of the cycle, an effect that was confirmed by analysing successive cycles without any averaging.

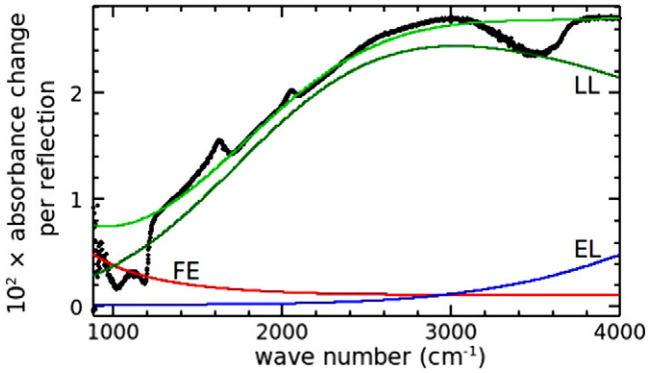

Fig. 8. Typical fit of the baseline (p-polarisation, t = 1800 s, *i.e.*, 900 s after the negative-potential step, with reference taken just before the negative potential step) as a superposition of an FE contribution (red), an LL contribution (dark green), and an EL (high-energy) contribution (blue). Experimental data as black dots, fit as light-green curve. The intervals 880–1260 cm^{-1}, 1350–1700 cm^{-1}, 2000–2150 cm^{-1}, 2500–3700 cm^{-1} have been excluded from the fit.

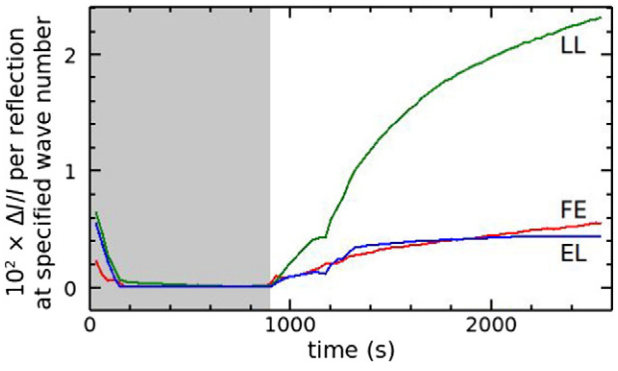

Fig. 9. s-p averaged baseline contributions (reference at t = 600–900 s, just before the negative potential step): FE specified at 1000 cm^{-1} (red), LL at 3000 cm^{-1} (green), and EL at 4000 cm^{-1} (blue). The shaded region indicates the time spent at the positive potential.

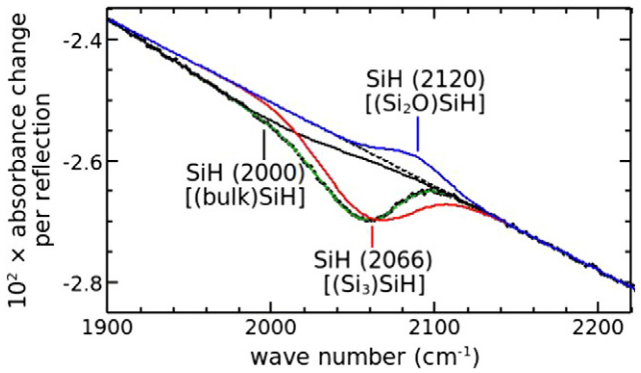

Fig. 10. Typical fit of the νSiH region with 3 Gaussian bands. Here $t = 900$ s (just before the negative potential step), p-polarisation, reference taken at the end of the cycle (fully hydrogenated surface).

3.2.2. νSiH region

Fig. 10 shows a narrow spectrum in the νSiH region, recorded at time $t = 900$ s, *i.e.* just before the negative-potential step. Besides the difference in the baseline (see above), this spectrum is significantly different from those measured at RT (Fig. 2a). Namely, in order to get a good fit, in addition to the two Gaussian bands at 2066 and 2120 cm^{-1}, it was found necessary to add a third Gaussian band SiH(2000), centred between 1990 and 2000 cm^{-1}. This extra band can be attributed to hydrogen in the Si lattice ("bulk" hydrogen) [26–29], an attribution consistent with its insensitivity to the polarisation. The variation of the three band intensities is shown in Fig. 11 (only p-polarisation shown). Though the fit is somewhat ill-conditioned [the SiH(2000) band possibly borrows some intensity from the Si(2066) band, as can be inferred from the plot of a linear combination of the two band intensities, see dashed curve in Fig. 11], it is clear that the new Si(2000) band has a time dependence distinct from that of the other two bands: it tends to increase steadily at the negative potential and its intensity at the end of the cycle is larger than at the beginning, a strong indication that hydrogen is incorporated into silicon at the negative potential. Note that the oxidised-SiH contribution SiH(2120) exhibits the same behaviour as for the RT data, namely, it is maximum in the regions where the SiH(2066) contribution changes (around $t = 150$ s and 1050 s), and it remains non-zero in the steady state at the positive potential. Finally, a marked difference with the RT data is the larger value of the band intensities (compare Figs. 3 and Fig. 11) and the reduced polarisation dependence of the SiH(2066) band (p/s ~ 3 instead of 10), which might suggest that potential cycling at 40 °C leads to significant roughening of the (111) surface. However, another explanation will be suggested later.

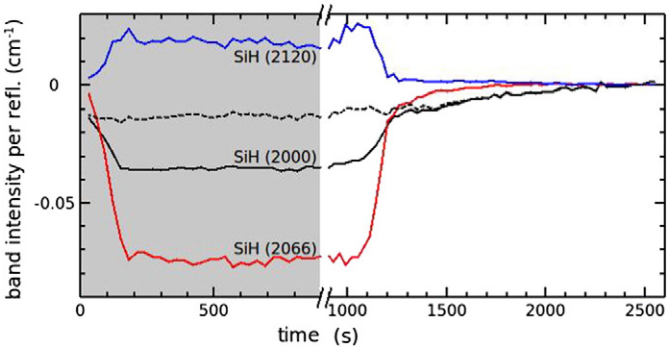

Fig. 11. Variation of the three SiH contributions. p-polarisation. The reference was taken at the end of the cycle (fully hydrogenated surface). The dashed line shows the intensity of the 2000 cm^{-1} band after subtraction of a fraction (0.3) of the intensity of the 2066 cm^{-1} band. Note that the only variation left is a slow increase at the negative potential. The shaded region indicates the time spent at the positive potential. Note the break in the time scale at the time of the negative potential step ($t = 900$ s).

4. Discussion

In this section, we will compare and discuss the results of the RT and 40 °C experiments. We will first consider the information that may be extracted from a quantitative analysis of the baseline, then the issues related to penetration of hydrogen into the silicon lattice. The detail of the variation of the two surface-SiH contributions [Si(2066) and Si(2120)], somewhat different at RT and at 40 °C, suggests that there is a delay associated with oxide nucleation, which is larger at 40 °C than at RT. These aspects will be addressed in the companion paper together with the issues related to the anodic current transient and the oxide formation/dissolution process [16].

4.1. Free-carrier contributions from the baseline

For the RT data, the free-carrier contributions can be analysed quantitatively. It appears that an electron accumulation layer with a concentration of 2.5 10^{13} cm^{-2} is present at the initial surface (before the positive potential step) and a hole inversion layer with a concentration of 8–10 10^{12} cm^{-2} is present in the steady state at the positive potential; this indicates the good electron-blocking properties of the oxide film. Note, however, that the latter figure may be an overestimate, because the scattering time of holes in such a high-concentration inversion layer may be significantly shortened as compared to its bulk value, thereby increasing their Drude-absorption cross-section.

Unfortunately, the free-carrier contribution in the 40 °C data is largely masked by the strong LL contribution, so that it is hardly possible to obtain any quantitative information from it. The best one can say is that the density of electrons in accumulation at the negative potential appears of the same order of magnitude as at RT (though possibly somewhat weaker).

4.2. Hydrogen penetration into the Si lattice

In the νSiH spectra at 40 °C, the presence of a low-energy band, whose intensity slowly increases while the potential is set negative, gives direct evidence that hydrogen is being incorporated into the silicon lattice [26–29]. We will see below that hydrogen incorporation occurs also at RT, though it is slower and this band is not visible in the spectra (see Fig. 2).

4.2.1. The RT results

At RT, the baseline includes a weak "constant" (wave-number independent) contribution and an exponential-like (EL) high-energy contribution. The "constant" contribution is maximum whenever the chemical state of the surface is changing, and it increases irreversibly during a cycle. The EL contribution decreases during formation of the oxide layer and increases after the oxide has been dissolved at the negative potential. We think that the "constant" contribution can be associated with light-diffusion losses induced by surface inhomogeneity (maximum during oxidation and oxide dissolution) and interface roughening (irreversible increase). It might be tempting to attribute the EL contribution to electronic surface-state absorption on the basis of similar spectral shapes reported in the literature [23]. However, the variations of this contribution during a cycle (increase at the negative potential and decrease at the positive potential) are just the opposite of those expected from surface states associated with oxide formation, such as reported in [23]. Here, a more plausible interpretation is that this EL absorption is due to an electronic transition associated with hydrogen inserted into the silicon lattice, and these electronic states are actually sub-surface states (located within the space-charge region or even beyond). There are several reports in the literature of hydrogen incorporation below the silicon surface in fluoride medium, including

during etching at OCP in NH_4F solution [30–32]. Here, it is plausible indeed to expect that the initial sample preparation leads to hydrogen incorporation. The variations of the EL contribution (Fig. 12a) upon successive potential cycling may then be explained by two competing phenomena: a progressive removal of the initial H-contaminated layer due to Si dissolution during each oxide formation/dissolution cycle and H-incorporation induced by the hydrogen evolution reaction at the negative potential, after complete oxide dissolution. The slow global decay of the EL component after each potential cycle indicates that H-incorporation is too "weak" to compensate the effect of Si dissolution. After a few cycles, the pre-existing H-contaminated layer is essentially etched away, which tends to lead to a periodic variation around a steady-state value (see the last cycle in Fig. 12a).

4.2.2. The 40 °C results

At 40 °C, the EL contribution undergoes similar variations, except that their amplitude is ~3 times larger than at RT (note that the cathodic current density is higher by a factor of ~30, compare Figs. 1 and 6) and the magnitude of the EL contribution seems to be recovered (within experimental uncertainty) at the end of a cycle. Furthermore, the most prominent Lucovsky-like (LL) contribution to the baseline appears. It undergoes variations qualitatively similar to those of the EL contribution. However, these variations present a much higher amplitude and are largely irreversible (the LL contribution increases upon potential cycling, see Fig. 12b). This suggests that the LL contribution is also due to hydrogen incorporation in another form, but now the amount of hydrogen incorporated at the negative potential exceeds that removed by etching at the positive potential, so that the amount of hydrogen stored in the silicon lattice increases during a cycle.

Assessing these interpretations would require a more precise knowledge of the form in which hydrogen is incorporated into the silicon lattice, together with information about the associated electronic levels. Though the information on the electrochemical incorporation of hydrogen into silicon is scarce, there is an extensive literature on hydrogen in silicon [33,34]: hydrogen may be present in silicon in the form of atomic H_1 or molecular H_2. In either case, it may be associated with defects (*e.g.*, vacancies, microvoids, self-interstitials) or other impurities (dopants, oxygen…). There is a wealth of data on the electronic levels associated with these various states, some of which are stable at low temperature only [33,34]. This opens a range of possibilities for the interpretation of our IR data.

4.2.3. Possible origins of the EL contribution

The exact origin of the EL contribution, common to both the RT and 40 °C data, will now be addressed. Its spectral shape, being not very characteristic, can be assigned to the low-energy tail of an optical transition between a level located deep in the band gap and either the conduction or the valence band. For example, if isolated-H_1 incorporation is considered (this is a plausible first step), an optical transition $H^- \rightarrow H^0 + e^-_{CB}$ might account for the observations under accumulation conditions since hydrogen would be in the form of H^- and the associated level H^-/H^0 is 0.62 eV below the conduction band [35]. Under depletion conditions, hydrogen would be in the form of H^+, and the optical transition $H^+ + e^-_{VB} \rightarrow H^0$ could be invoked (H^0/H^+ is 0.94 eV above the valence band [35]). Note that hydrogen at the Si–Si bond-centre position is known to lead to a vibrational band at 1998 cm^{-1} [36], which would match our observations. However, such centres are unstable at room temperature because they can diffuse and undergo pairing as H_2 molecules at the tetrahedral interstitial site (so-called H_2^T centres) or as H^+ and H^- at two neighbouring Si sites (so-called H_2^* centres) [35,37]. Isolated-H_1 centres can then be considered only as a low-concentration species or as a transient state. It is equally plausible that the EL contribution arises from states associated with H_2^T or H_2^* centres, whose energy levels are not known with certainty. Note that, based on interface capacitance data on a hydrogen-loaded silicon electrode, Jakob and Schindler [32] have reported three levels in the range from 0.3 to 0.5 eV below the conduction band, which is not inconsistent with our observations.

In any case, none of these species can account for the SiH(2000) band (the concentration of H_1 centres cannot be large enough and the H_2 species do not match the spectrum). Another origin must then be sought for this band, which from its variation (Fig. 11) seems rather related to the LL contribution.

4.2.4. Possible origins of the LL contribution

The shape of the LL contribution is more characteristic, and the values extracted from the fits based on Lucovsky's model indicate a threshold energy of 0.2 ± 0.04 eV with an r.m.s. broadening of 50 ± 12 meV, and an areal concentration on the order of 10^{15} cm^{-2}. The latter figure is definitely too high to allow for the possibility of a charged centre. One must then think of a neutral level that would be either a donor near the conduction band or an acceptor near the valence band. Neutral hydrogen at the Si–Si midbond position would match these requirements (H^0/H^+ level is 0.16 eV below conduction band, with a weak reorganisation expected [35]). However, the single-hydrogen centre in silicon is a negative-*U* centre, so that the number of sites in the 0-charge state is always orders of magnitude smaller than the total number of these centres, which clearly rules out this interpretation. We have considered various other possible attributions, including that of metal contamination from the stainless-steel counter electrode due to

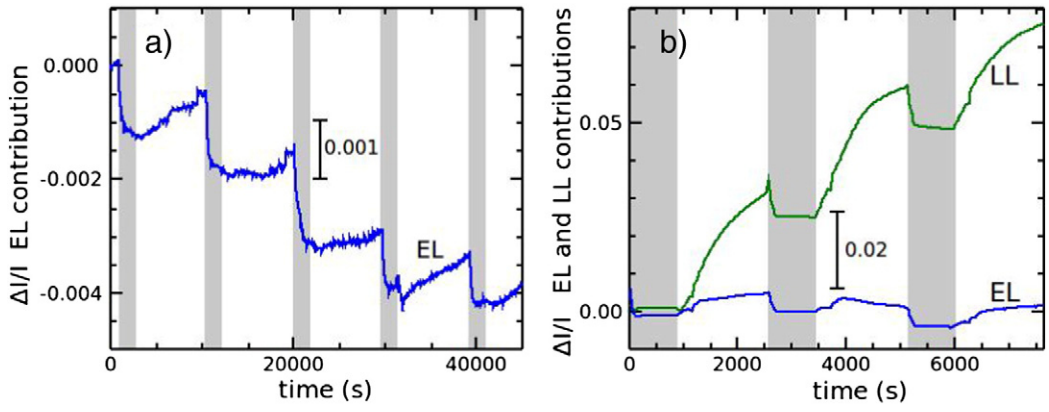

Fig. 12. Behaviour of the EL contribution (blue, specified at 4000 cm^{-1}) and LL contribution (green, specified at 3000 cm^{-1}) over several cycles, at RT (a) and at 40 °C (b). Average of the s- and p-polarised spectra. The reference spectrum is that of the first cycle. The shaded regions mark the times spent at the positive potential. Note that the vertical scales in the two frames differ by an order of magnitude. At RT, there is no LL contribution, and the EL contribution is seen to decrease upon potential cycling. At 40 °C, upon potential cycling, the EL contribution appears essentially stable whereas the LL contribution steadily increases.

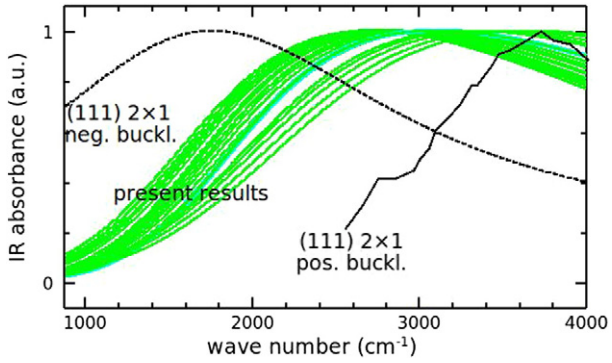

Fig. 13. Absorption shape of our LL contribution (green, various curves superimposed, corresponding to the various parameter sets used for fitting our data) compared to the absorption shape of surface states at the (111) 2 × 1 clean surface ([39], solid black) and the calculated absorption shape for the negative-buckling isomer configuration ([42], dashed black). The curves have been scaled so that their maximum is unity.

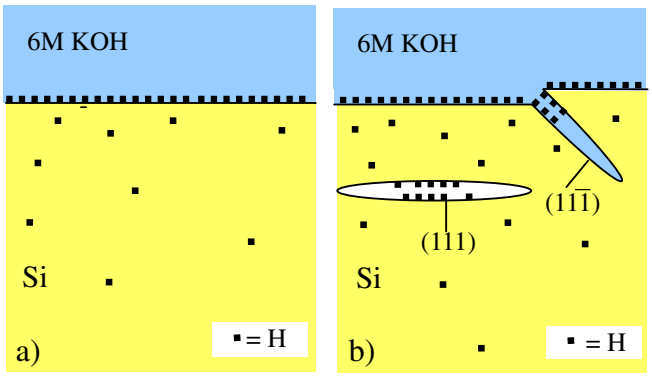

Fig. 14. Proposed scheme for the electrochemical hydrogen incorporation into silicon. (a) As a first step, hydrogen is incorporated as isolated centres (H_1, H_2^T, or H_2^*), responsible for the EL absorption; (b) at high hydrogen loading (a situation reached here at 40 °C), the accumulation of stress leads to the formation of (111)-oriented microcracks whose surface acts as a trap for any further incorporated hydrogen. The partially hydrogen-decorated surface accounts for the enhanced νSiH absorption and the LL absorption (π–π* transition at the non-hydrogenated locations).

potential cycling. However, as mentioned in Section 2, no such contamination on our samples was detectable by XPS. Also, one may note the similarity of this spectrum with that due to transitions between Urbach-bandtail states and delocalised states in amorphous hydrogenated silicon [38]. However, in contrast to [28], we regard it as unlikely that the silicon lattice is perturbed by hydrogen incorporation to the extent of amorphous silicon formation (which would undergo fast chemical dissolution in 6 M KOH, thereby ruining the anisotropic dissolution properties). Among the numerous vacancy-hydrogen complexes reported in the literature, we have found none satisfying the above requirements, because their donor levels are generally located at an energy lower than that of their acceptor levels, which makes the possible transition energies much larger than 0.2 eV. Finally, the phosphorus–hydrogen complexes are not stable at RT and cannot be invoked here [35].

From the above, it seems that the LL contribution calls for another interpretation. It should be noted that IR absorption by localised states is not limited to transitions between a localised state and either the conduction or the valence band, but processes within the localised states are also possible. In particular, a π–π* transition between two surface-state bands is known to be responsible for the IR absorption observed at the Si (111) 2 × 1 surface obtained by cleavage in UHV [39–41]. The corresponding optical cross-section is fairly large (~10^{-16} cm^2). Fig. 13 shows the corresponding spectral shape together with the LL shape used here to fit our spectra. Though Lucovsky's model is not relevant for such a transition and the similarity between the two spectral shapes is more qualitative than quantitative, it is tempting to attribute our LL contribution to such a process. This hypothesis is supported by the expectation that the energy of maximum absorption at the (111) 2 × 1 surface depends on the π–π* splitting, which is itself predicted to depend on the detail of the atomic reconstruction, namely, the sign of the π-chain buckling, see *e.g.*, dashed line in Fig. 13 [42]. Interestingly, while positive buckling is the normally stable configuration, it has been found that negative-buckling regions may coexist with positive buckling at high electron concentrations [43,44], such as those present at our strongly accumulated surface.

4.2.5. Proposed scenario

The discussion above then leads us to propose the following scenario: hydrogen loading first takes place in the form of single-hydrogen atoms, which pair as H_2^T and/or H_2^* centres, either of these species being responsible for the EL absorption (Fig. 14a). Upon strong hydrogen loading at 40 °C, the concentration of H_2^T and/or H_2^* centres reaches a critical value which cannot be exceeded (solubility limit): upon further hydrogen incorporation, the associated stresses lead to the formation of microcracks which can accept extra hydrogen atoms at their surface (Fig. 14b). The formation of microvoids in the form of (111)-oriented platelets is indeed known to take place at silicon surfaces exposed to proton bombardment or a hydrogen plasma [45–47]. Here, this process may account for most of the features (larger νSiH intensity with reduced polarisation dependence, increase in the "constant" baseline contribution) which were initially ascribed to roughening. It also supplies a more satisfactory interpretation of the historical ellipsometric data of Palik et al. [48], which had tentatively been analysed in terms of an SiO_x "slush layer" (at that time it was not known that the Si surface at OCP is hydrogen terminated). One may infer that the walls of the microcracks will be partly covered with hydrogen. The 2 × 1 reconstruction is reported to be stable up to a hydrogen coverage of *ca* 0.3 [49]. The bare parts are expected to be similar to a cleaved Si surface, exhibiting a π-π* electronic transition responsible for the observed LL contribution, whereas the hydrogen-decorated parts account for an increased νSiH absorption. The latter may appear in two forms: i) superimposed on the main band (for places where the 2 × 1 reconstruction is lifted), accounting for its larger intensity and reduced polarisation dependence as compared to the RT data, and ii) under the form of the 2000 cm^{-1} band (for places where the 2 × 1 reconstruction survives). The low energy of this band as compared to that of the "standard" monohydride on a flat (111) surface may be attributed to a larger bond angle of the Si–Si backbonds in the π-bonded chains, which gives the Si orbital pointing towards the hydrogen a *p* rather than sp^3 character [50]. The possibility that the incorporated hydrogen diffuses through the space-charge region and reaches the neutral region cannot be ruled out, but our data do not provide evidence about that point.

In conclusion, we regard as a plausible mechanism the incorporation of hydrogen in single-atom form, followed by its transformation into H_2^T or H_2^*. The increase in concentration of such defects leads to the formation of microcracks partially decorated with hydrogen.

4.2.6. Hydrogen evolution reaction

Finally, we are now in a position to discuss the origin of the large increase in the hydrogen-evolution current when the potential is kept at its negative value. The initial increase in cathodic current is obviously associated with dissolution of the oxide and regeneration of the hydrogenated surface, but the persistent increase at long times (t > 7000 s, see Fig. 1b, or t > 1200 s, see Fig. 6b) is clearly due to another mechanism.

We think that two extra mechanisms are actually present. The increase in specific surface area associated with the formation of microcracks may obviously account for part of the current increase, especially that at t > 1400 s at 40 °C. However, unlike the increase in specific surface area, a long-term increase in cathodic current is

present at RT as well as at 40 °C. We then conclude that a second mechanism must be sought, which is associated with the hydrogen incorporated in the form of isolated sub-surface centres. On general grounds, a current increase may proceed either through a decrease in band bending, leading to a higher electron concentration at the surface, or through a catalytic effect of the centres located within atomic distance from the surface. However, the surface is known to be under strong electron-accumulation conditions and the free-electron absorption does not seem to increase after regeneration of the SiH surface (see Fig. 5a, $t > 7000$ s). We then think that the first kind of effect is hardly operative, and a catalytic effect through near-surface centres (H_1, or more probably H_2^* or H_2^T) appears as the most plausible mechanism.

5. Conclusion

A detailed analysis of real-time IR data recorded during oxide formation/dissolution cycles indicates that the silicon surface is under strong accumulation at the negative potential. It converts to depletion when the potential is stepped positive, and an inversion layer appears after a delay. The hydrogen termination of the surface is destroyed at the positive potential and regenerated after an induction time at the negative potential. Finally, our detailed analysis of the baseline and νSiH region provides strong evidence of hydrogen incorporation into the silicon lattice at the negative potential. We suggest a mechanism for this incorporation. Hydrogen penetration appears to be faster at higher temperature, and the accumulation of hydrogen in the silicon lattice leads to the formation of microcracks partially decorated with hydrogen atoms. This point is important, because it indicates that, in contrast to naive expectation, the chemistry and morphology of the silicon surface in aqueous medium can undergo dramatic changes even when keeping the potential negative.

Acknowledgments

The authors are indebted to Dr D. Aureau, from Université de Versailles–St Quentin en Yvelines, for kindly checking for the absence of metal contamination on our samples by XPS. One of us (HGGP) thanks the Dutch Technology Foundation (STW, TPC-5990) for supporting his stay at Ecole Polytechnique.

Appendix A. Details of the fitting procedures used in this work

A.1. General principles

Our fitting software allows one to fit the spectra in a given spectral window (possibly excluding some intervals within this window), as the linear superposition of i) several pseudo-Voigt functions simulating the vibrational bands (up to 4 adjustable parameters each), ii) a "generalised trinomial" baseline (*i.e.*, $a\sigma^{\alpha} + b\sigma^{\beta} + c\sigma^{\gamma}$, where a, b, c, α, β, γ may be arbitrary real numbers: up to 6 adjustable parameters), iii) and several "component spectra" recorded independently in the same window (1 adjustable parameter each). Though this software might allow one to fit the whole spectral range in a single operation, the results here were found to be very sensitive to the fitting of the baseline (quite important in these experiments), and better results on the vibrational bands were obtained by fitting them in a narrow region with a "local" baseline, the "full-range" baseline being fitted separately by excluding the regions in which vibrational bands are present. The possibility of including component spectra as inputs to the fit was especially helpful in three instances: i) to represent the loss in electrolyte absorption associated with oxide film growth (electrolyte absorption used as a component spectrum, see [16]), ii) to fit the free-carrier absorption (see below), iii) to correct for problems associated with detector non-linearity (see [16]).

A.1.1. Free-carrier absorption

In the framework of the Drude model, the complex dielectric function of a free-electron gas at frequency $\omega/2\pi$ is given by $\varepsilon(\omega) = \varepsilon_\infty - i\sigma(\omega)/\varepsilon_0\omega$ where $\sigma(\omega) = ne^2\tau/m(1 + i\omega\tau)$ is the complex conductivity and τ is the electron scattering time. In the IR range, one can use the approximation $\omega\tau >> 1$; hence, the IR absorption is proportional to $-\omega\,\mathrm{Im}[\varepsilon(\omega)] = ne^2/m\varepsilon_0\omega^2\tau$. This absorption is seen to increase at long wavelengths (small ω) as ω^{-2}. However, due to the energy dependence of τ, the exponent of the power law may actually differ from -2 [51]. Absorption by holes in silicon is a good example of a pure Drude behaviour, the exponent being close to -2 [52].

In the presence of a complex band structure, interband transitions may fall in the IR range and contribute to IR absorption. Such is the case for n-Si [53,54], for which an empty branch of the conduction band is present about 0.5 eV above the conduction-band minimum along the ΓX direction of the first Brillouin zone. In practice, free-electron absorption in n-Si, as originally determined by Spitzer and Fan (SF) [53], can be reproduced as the sum of a power law (Drude contribution: DC) and a Gaussian shape (interband contribution: IBC): $A/\sigma^B + C\exp(-(\sigma - D)^2/2E^2)$, with $A = 0.475 \times 10^7$ cm^{-2}, $B = 2$, $C = 1.5$, $D = 3800$ cm^{-1}, and $E = 1500$ cm^{-1}. However, near the surface, and especially in an accumulation layer of high surface concentration, the electron scattering time is shortened, which leads to an increase of the DC/IBC ratio [55,56] as compared to the original Spitzer-Fan data. The expected ratio in an accumulation layer of surface concentration n_S is expected to follow a law DC/IBC $\propto 1/\tau \propto 1 + (n_S/n_{S0})^{1/3}$, where $n_{S0} \sim 10^{11}$ cm^{-2} [55,56]. Free-electron absorption in an accumulation layer can then be represented as the sum of an SF shape (implemented as a component spectrum) plus an extra power-law contribution with exponent -2, its coefficient a_{DC} (proportional to $n_S \times n_S^{1/3}$) being tied to that of the SF contribution a_{SF} (proportional to n_S) through a relation $a_{DC} = \mathrm{cst}\ a_{SF}^{4/3}$ (a DC exponent of -2 was kept for simplicity, though a value of $-3/2$ at high accumulations has been reported [55]; this choice is not critical due to the strong overlap with the IBC, whose neglect in [55] may actually have led to a biassed result).

A.2. Conditions used for fitting specific spectral regions

A.2.1. Baseline

For the RT data, a simple examination of the spectra at low wave number indicates the presence of a large negative FC contribution appearing immediately after the positive-potential step. The magnitude of this signal suggests that, at the negative potential, an electron-accumulation layer with an electron density on the order of 10^{13} cm^{-2} may be present. Furthermore, the weak increase of the baseline some time after the positive potential step suggests that a hole inversion layer may appear in the presence of oxide. We have then modelled the free-carrier contribution as follows.

At the positive potential, the sum of three components was used: i) a negative SF contribution SF1 with the normal DC/IBC ratio, the amplitude a_{SF1} (<0) being the only adjustable parameter; ii) a negative Drude contribution DC1 with an amplitude a_{DC1} determined from a_{SF1}, according to the law $|a_{DC1}| = \mathrm{cst}\ |a_{SF1}|^{4/3}$, representing the extra Drude absorption of electrons in a high-density accumulation layer,[3] iii) a positive Drude contribution DCh with adjustable amplitude a_{DCh}, representing hole absorption in an inversion layer. In a first step, a_{SF1} was left free. The resulting variation appeared as a noisy negative-going step, as may be expected from the loss of the accumulation layer (present at the negative potential only). In a second step, a_{SF1} was frozen at its average value, leaving a_{DCh} as the only free parameter

[3] The constant was determined from the fits of the first few spectra following the positive-potential step, for which the free-hole contribution is negligible, and was kept constant for the following fits. The obtained value amounts to taking $1/\tau \propto 1 + \xi n_S^{1/3}$, with $\xi \approx 0.5\ 10^{-4}$ cm$^{2/3}$, a reasonable figure though somewhat smaller than expected [55,56].

for the free-carrier contribution. At the negative potential, no hole absorption is to be expected, but electron accumulation is expected to reappear. Therefore, the above (frozen) components i) and ii), corresponding to the loss of the initial free-carrier absorption, were kept, and component iii) was replaced by iii) another (positive) SF contribution with amplitude a_{SF2}, and iv) the corresponding extra Drude absorption $a_{DC2} = \text{cst}\, a_{SF2}^{4/3}$ (a_{SF2} being the only free parameter). The actual accumulated free-electron contribution is then represented by the algebraic sum $a_{SF1} + a_{SF2}$.

For the 40 °C data, the weak free-carrier contribution was built in the same way as for the RT data (SF shape plus extra Drude component proportional to $|a_{SF}|^{4/3}$), but the baseline appears dominated by a Lucovsky-like contribution. This shape was implemented in the fitting routine as the sum of 7 Gaussian curves $\Sigma_k\, a_k \exp[-(\hbar\omega - E_k)^2/2(\lambda E_k)^2]$, with only 3 free parameters, the parameters (centre and amplitude) of the last 6 Gaussians being proportional to those of the first one (the proportionality coefficients being determined from a fit of the actual Lucovsky shape). Keeping the width of each Gaussian proportional to its centre value (single free parameter λ) allows for a possible broadening of the original Lucovsky shape in the presence of atomic reorganisation effects.

A.2.2. νSiH region

For the RT data, the νSiH spectrum was fitted in the interval 1900–2300 cm^{-1}, as a second-order polynomial baseline (3 parameters) plus two Gaussian contributions (3 parameters each, namely, centre, FWHM, and amplitude). At a first stage, the fits were made by leaving all 9 parameters free, leading to noisy results and sometimes instability of the fit. In a second stage, the centre and FWHM of the main Gaussian were fixed at their average values (2065.7 and 46 cm^{-1}, respectively) and the fit was made with 7 free parameters. For the 40 °C data, a third Gaussian contribution was added, and for the final fit, its position and FWHM were fixed at 2000 and 110 cm^{-1}, respectively.

References

[1] H. Seidel, L. Csepregi, A. Heuberger, H. Baumgärtel, J. Electrochem. Soc. 137 (1990) 3612.
[2] P. Allongue, V. Costa-Kieling, H. Gerischer, J. Electrochem. Soc. 140 (1993) 1018.
[3] R.A. Wind, H. Jones, M.J. Little, M.A. Hines, J. Phys. Chem. B 106 (2002) 1557.
[4] Q.D. Nguyen, M. Elwenspoek, J. Electrochem. Soc. 154 (2007) D684.
[5] S.D. Collins, J. Electrochem. Soc. 144 (1997) 2242.
[6] J.J. Kelly, X.H. Xia, C.M.A. Ashruf, P.J. French, IEEE Sensors J. 1 (2001) 127.
[7] A.J. Nijdam, E. van Veenendaal, J.G.E. Gardeniers, A.P.M. Kentgens, G.H. Nachtegaal, M. Elwenspoek, J. Electrochem. Soc. 147 (2000) 2195.
[8] W. Haiss, P. Raisch, D.J. Schiffrin, L. Bitsch, R.J. Nichols, Faraday Discuss. 121 (2002) 167.
[9] J. Rappich, H.J. Lewerenz, H. Gerischer, J. Electrochem. Soc. 140 (1993) L187.
[10] P. Allongue, H. Brune, H. Gerischer, Surf. Sci. 275 (1992) 414.
[11] H.G.G. Philipsen, J.J. Kelly, J. Phys. Chem. B 109 (2005) 17245.
[12] X.H. Xia, C.M.A. Ashruf, P.J. French, J. Rappich, J.J. Kelly, J. Phys. Chem. B 105 (2001) 5722.
[13] X.H. Xia, J.J. Kelly, Phys. Chem. Chem. Phys. 3 (2001) 5304.
[14] H.G.G. Philipsen, N.J. Smeenk, H. Ligthart, J.J. Kelly, Electrochem. Solid-State Lett. 9 (2006) C118.
[15] R.L. Smith, B. Kloeck, S.D. Collins, J. Electrochem. Soc. 135 (1988) 2001.
[16] H.G.G. Philipsen, F. Ozanam, P. Allongue, J.J. Kelly, J.-N. Chazalviel, submitted for publication.
[17] J.-N. Chazalviel, B.H. Erné, F. Maroun, F. Ozanam, J. Electroanal. Chem. 509 (2001) 108.
[18] C. da Fonseca, F. Ozanam, J.-N. Chazalviel, Surf. Sci. 365 (1996) 1.
[19] M.L. Munford, R. Cortès, P. Allongue, Sens. Mater. 13 (2001) 259.
[20] G.S. Higashi, Y.J. Chabal, G.W. Trucks, K. Raghavachari, Appl. Phys. Lett. 56 (1990) 656.
[21] F. Ozanam, A. Djebri, J.-N. Chazalviel, Electrochim. Acta 41 (1996) 687.
[22] G. Lucovsky, Solid State Commun. 29 (1979) 571.
[23] J.-N. Chazalviel, A. Venkateswara Rao, J. Electrochem. Soc. 134 (1987) 1138.
[24] G. Lucovsky, Solid State Commun. 3 (1965) 299.
[25] P. Atkins, J. de Paula, Elements of Physical Chemistry, sixth ed. Oxford University Press, Oxford, UK, 2013 507.
[26] K.C. Mandal, F. Ozanam, J.-N. Chazalviel, Appl. Phys. Lett. 57 (1990) 2788.
[27] P. de Mierry, A. Etcheberry, M. Aucouturier, J. Appl. Phys. 69 (1991) 1099.
[28] P. de Mierry, A. Etcheberry, R. Rizk, P. Etchegoin, M. Aucouturier, J. Electrochem. Soc. 141 (1994) 1539.
[29] A. Belaïdi, J.-N. Chazalviel, F. Ozanam, O. Gorochov, A. Chari, B. Fotouhi, M. Etman, J. Electroanal. Chem. 444 (1998) 55.
[30] P. Allongue, C. Henry de Villeneuve, M.C. Bernard, J.E. Péou, A. Boutry-Forveille, C. Lévy-Clément, Thin Solid Films 297 (1997) 1.
[31] D. Aureau, PhD thesis, École Polytechnique, France, 2008. https://pastel.archives-ouvertes.fr/pastel-00004611/document (last accessed April 2015).
[32] S. Jakob, W. Schindler, Electrochim. Acta 88 (2013) 659.
[33] J.I. Pankove, N.M. Johnson (Vol. Eds.), Hydrogen in Semiconductors, Semiconductors and Semimetals, vol. 34, R.K. Williardson, A.C. Beer (Eds.), Academic Press Inc., San Diego, CA, 1991.
[34] S.J. Pearton, J.W. Corbett, M. Stavola, Hydrogen in Crystalline Semiconductors, Springer Series in Materials Science, vol. 16, Springer-Verlag, Berlin/Heidelberg, Germany, 1992 (Chap. 11).
[35] C. Herring, N.M. Johnson, C.G. Van de Walle, Phys. Rev. B 64 (2001) 125209.
[36] M. Budde, G. Lüpke, C. Parks Cheney, N.H. Tolk, L.C. Feldman, Phys. Rev. Lett. 85 (2000) 1452.
[37] J.D. Holbech, B. Bech Nielsen, R. Jones, P. Sitch, S. Öberg, Phys. Rev. Lett. 71 (1993) 875.
[38] K. Rerbal, J.-N. Chazalviel, F. Ozanam, I. Solomon, Phys. Rev. B 66 (2002) 184209.
[39] G. Chiarotti, S. Nannarone, R. Pastore, P. Chiaradia, Phys. Rev. B 4 (1971) 3398.
[40] K.C. Pandey, Phys. Rev. Lett. 47 (1981) 1913.
[41] P. Chiaradia, A. Cricenti, S. Selci, G. Chiarotti, Phys. Rev. Lett. 52 (1984) 1145.
[42] C. Violante, A. Mosca Conte, O. Pulci, J. Phys. Conf. Ser. 383 (2012) 012015.
[43] G. Bussetti, B. Bonanni, S. Cirilli, A. Violante, M. Russo, C. Goletti, P. Chiaradia, O. Pulci, M. Palummo, R. Del Sole, P. Gargiani, M.G. Betti, C. Mariani, R.M. Feenstra, G. Meyer, K.H. Rieder, Phys. Rev. Lett. 106 (2011) 067601.
[44] R.M. Feenstra, G. Bussetti, B. Bonanni, A. Violante, C. Goletti, P. Chiaradia, M.G. Betti, C. Mariani, J. Phys. Condens. Matter 24 (2012) 354009.
[45] N.M. Johnson, F.A. Ponce, R.A. Street, R.J. Nemanich, Phys. Rev. B 35 (1987) 4166.
[46] A.W.R. Leitch, J. Weber, V. Alex, Mater. Sci. Eng. B 58 (1999) 6.
[47] N.H. Nickel, G.B. Anderson, N.M. Johnson, J. Walker, Phys. Rev. B 62 (2000) 8012.
[48] E.D. Palik, V.M. Bermudez, O.J. Glembocki, J. Electrochem. Soc. 132 (1985) 871.
[49] F. Ancilotto, A. Selloni, Phys. Rev. Lett. 68 (1992) 2640.
[50] M. Budde, Ph.D. thesis, Aarhus University, Denmark, 1998. http://phys.au.dk/fileadmin/site_files/publikationer/phd/Michael_Budde.pdf (last accessed April 2015).
[51] J.I. Pankove, Optical Processes in Semiconductors, Prentice-Hall, Englewood Cliffs, NJ, 1971 74.
[52] H. Hara, Y. Nishi, J. Phys. Soc. Jpn. 21 (1966) 1222.
[53] W. Spitzer, H.Y. Fan, Phys. Rev. 108 (1957) 268.
[54] A. Venkateswara Rao, J.-N. Chazalviel, F. Ozanam, J. Appl. Phys. 60 (1986) 696.
[55] A. Tardella, J.-N. Chazalviel, Phys. Rev. B 32 (1985) 2439.
[56] H. Benisty, J.-N. Chazalviel, Phys. Rev. B 41 (1990) 12568.